Comparisons Between ATSR Derived SSTs and AVHRR SSTs

J.Vazquez and R. Sumagaysay
Physical Oceanography Distributed Active Archive Center, Jet Propulsion Laboratory
California Institute of Technology
4800 Oak Grove Dr. M/S 300/323
Pasadena, California, USA 91109
jv@pacific.jpl.nasa.gov

INTRODUCTION

Water vapor and aerosols are two major sources of error in the algorithms used to measure sea surface temperatures (SST) from the Advanced Very High Resolution Radiometer (AVHRR) and the Along Track Scanning Radiometer (ATSR) (Murray et al., 1996; Emery et al., 1994; May et al., 1992) on-board the European Remote Sensing Satellite (ERS1). In addition, biases in the data may exist due to the differences in the skin and bulk SST (Schluessel, 1990l; Anyamba, E., and J. Susskind, 1998). Differences between the SSTs measured by these two instruments can be attributable to skin-bulk temperature differences, as well as possible cloud contamination, aerosols and water vapor.

The AVHRR instrument is a 5 channel radiometer with three channels in the infrared and two channels in the visible spectrum (see table 1).

Current retrieval algorithms for sea surface temperature from AVHRR are based largely upon the multi-channel sea surface temperature (MCSST) algorithm (McClain et al., 1985) which may be written as:

$$SST=\alpha_1 + a_2T_4 + \gamma (T_4 - T_5) \qquad (1)$$

where α_1 and α_2 are constants determined through a least-squares fit to in-situ data, T_4, T_5, are brightness temperatures as derived from channels 4 and 5 and γ is a weighting factor based on the knowledge of known absorption coefficients (Emery et al., 1994). A non-linear form (NLSST) of the algorithm was introduced which also incorporated an initial guess field. The form of the NLSST algorithm becomes:

$$SST=\alpha_1 + a_2T_4 + \alpha_3 (T_4 - T_5)*T_{surf} + \alpha_4 (\sec(\theta)-1)(T_4 - T_5) \qquad (2)$$

where the "α_s" are still coefficients based on a least squares fit to in-situ data and T_4, T_5 are the brightness temperatures in channels 4 and 5. Theta is the satellite scan angle and T_{surf} is a first guess sea surface temperature field; in this case the Reynolds optimally interpolated sea surface temperature data. A modification in this algorithm, where the yearly coefficients are calculated for three different water vapor regimes, was introduced into the NLSST formulation. This form of the modified Pathfinder algorithm (MPFSST) was approved for processing of the version 1.0 NOAA/NASA AVHRR Oceans Pathfinder Data.

Version 1.0 of the algorithm was found to not

perform adequately (Robert Evans, personal communication) during times of high aerosol content, such as the eruption of Mt. Pinatubo. In version 3.0 of the algorithm, monthly coefficients were calculated over 5 month running means. The coefficients were calculated for $T_4 - T_5 < 0.7$ and $T_4 - T_5 > 0.7$. This form of the algorithm (version 3.0) was approved for the reprocessing of the AVHRR data by the AVHRR Oceans Science Working group because it tended to lower the overall bias over the widest possible environmental conditions (Evans and Podesta, 1996). Further modifications of the algorithm (version 4.0) included the implementation of a tree algorithm to define a series of quality flags Guillermo Podesta and Katherine Kilpatrick, personal communication)

Unlike the AVHRR, the ATSR instrument has 4 channels (Murray et al., 1996) (see table 1) and has dual view capability. The latter three bands are in the infrared range. For both the AVHRR and ATSR instruments, the correction for aerosols is difficult to define due to the differences in the sizes, compositions, concentrations and temporal variability of the aerosols (May et al., 1992). Water vapor also acts to attenuate the signal and has been incorporated into models of sea surface temperature (Emery et al., 1994). SSTs from the ATSR instrument are derived from a combination of observed brightness temperatures in the infrared range or:

$$SST = a_o + \sum a_i T_i$$

where a_i are coefficients calculated from a fit to a radiative transfer model, instead of in-situ observations, as in the NLSST

DATA AND PROCESSING

To compare directly the ATSR derived SSTs with the AVHRR derived SSTs it was necessary to bin the data to the same space-time grid. This was done by simply binning both SST data sets to a weekly, one degree grid and then calculating average differences. A third data set, the matchup data set from the Pathfinder SST calculation, was also used in the comparison. Mean differences and root mean square differences (rmsd) were calculated between the matchup in-situ measurements of SST and the ATSR (ASST) , AVHRR (PSST) derived SSTs. Data for the ASST and the PSST were compared between 1992 and 1996.

RESULTS

Figure 1 shows the longitudinally averaged differences for ASST-PSST . Regions of purple and blue indicate negative differences can exceed 2° with the ASST cooler than the PSST. In addition an annual cycle is clearly visible in the mid to high latitudes.

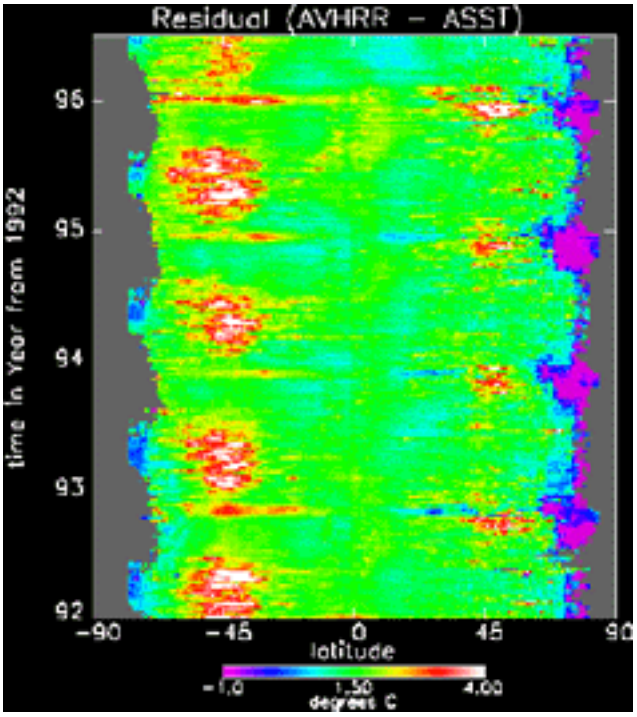

Figure 1-Zonal averages for PSST-ASST for 1992-1996. Color Scale ranges from -1 degrees to 4 degrees Celsius. Purple indicate negatives values and white indicate differences around 4 degrees..

Figure 2 (a,b) shows the SST variability using PSST and the ASST. Similarities exist in that both show high variability in the areas of the western boundary currents. These areas show variability of > 5°. Both the ASST and the PSST show high variability in the middle latitudes where the annual cycle is expected to dominate.

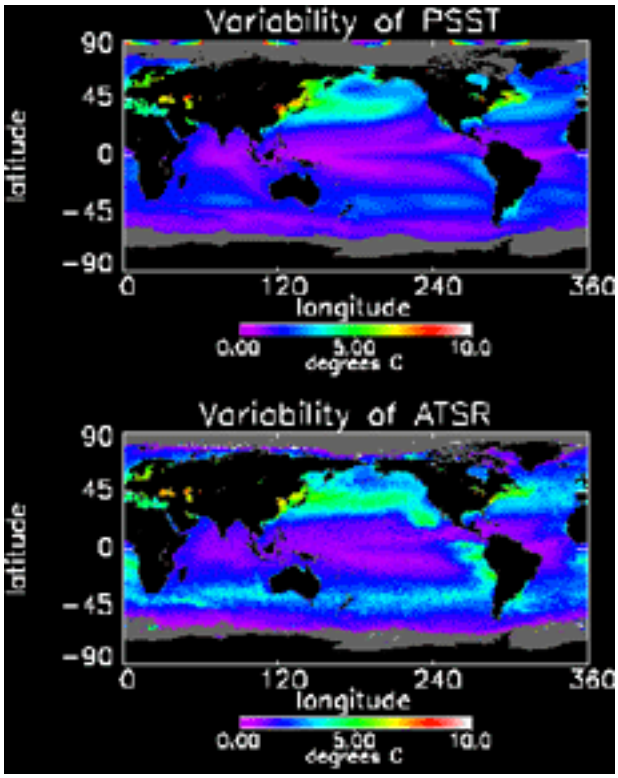

Figure 2-Variability in degrees Celsius for PSST and ASST. Highest values are green to red and are approximately 5 degrees Celsius.

Figure 3(a,b) shows the temporally averaged differences (PSST-ASST) between 1992-1996 for the entire Earth. Areas of high positive differences (>3 degrees Celsius) are associated with areas of high variability indicating that the ASST is measuring a cooler temperature than the PSST. In addition an area of large positive values (3 degrees Celsius) is also clearly visible at 45S.

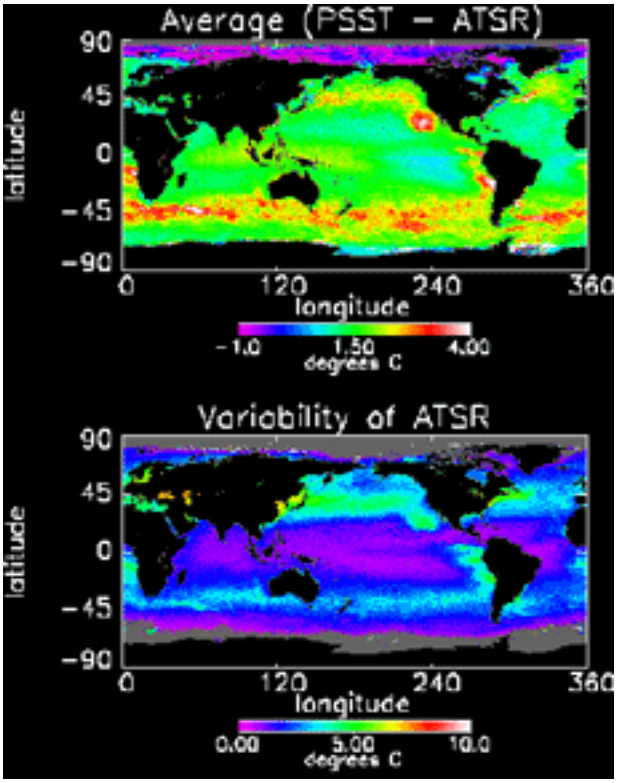

Figure 3-Global Map of Average difference between PSST-ASST for 1992-1996.

Red to white values indicate positive differences (PSST warmer than ASST). Bottom Map shows the Variability of ASST for comparison.

In order to extract the time-space scales of the PSST-ASST differences a set of empirical orthogonal functions were determined. Figure 4(a,b) shows the spatial structure of the first and second EOFS of the ASST-PSST differences. Large differences are visible in areas of the western boundary currents associated with the Kuroshio and Gulf Stream Extensions. In addition, large differences are seen off the coast of Peru, California and at 45S.

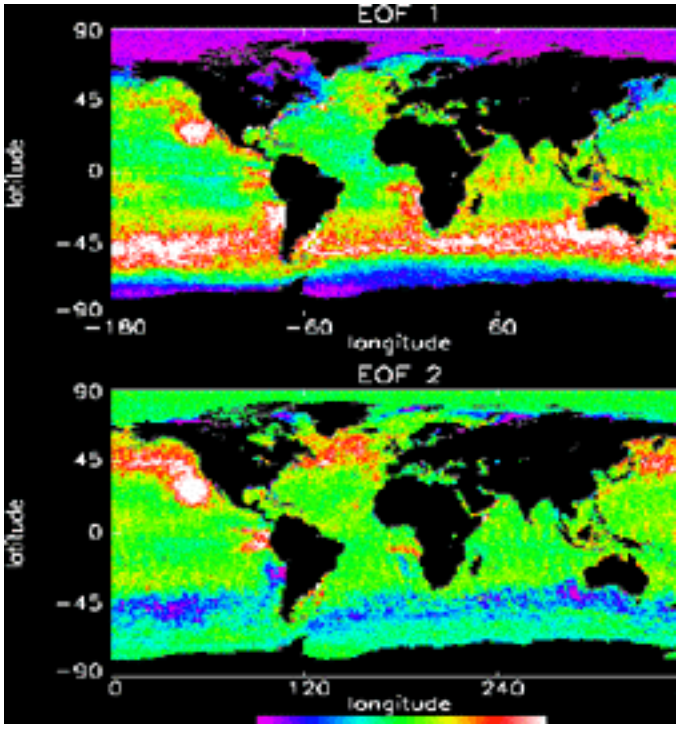

Figure 4-Spatial structure of first two EOFs of PSST-ASST

Figure 5(a.,b,c) shows the time series for the first

three EOF modes (see end of article). The first two modes are clearly associated with an annual cycle. The first mode indicates that maxima are occurring in the mid-late winter time frame. Thus the large differences between PSST and ASST at 45S, and off the coasts of South America, and South Africa, are at a maxima in the mid-late winter time frame. The second EOF 6(b) shows a time series that has an annual cycle with a maxima in the mid to late summer time frame and a minimum in the winter. The opposite sign between the Northern and Southern Hemisphere indicates that a possible cause for this mode lies in the seasonal heating and cooling of the ocean surface. The third mode also appears to be associated with an annual cycle with maxima in the summer.

All the EOFs indicate that differences between the ASST and PSST measured SST may exceed 3 degrees.

COMPARISONS WITH MATCHUP DATABASE

The following two tables show the statistics for the differences between the PSST, ASST and the in-situ data from the Pathfinder Matchup Database. The statistics are calculated for the global oceans (Global), North Atlantic (NA), South Atlanticf (SA), North Pacific (NP), South Pacific (SP), and the Indian Ocean. Two statistics are shown the mean difference and the root mean square difference (RMSD).

TABLE 1

Statistics for PSST- In - Situ

Basin	Mean Difference	RMSD
Global	-0.22	0.42
NA	0.14	0.47
SA	-0.54	0.71
NP	-0.34	1.05
SP	-0.24	1.42
Indian	-0.60	0.88

TABLE 2

Statistics for ASST-In-Situ

Basin	Mean Difference	RMSD
Global	-0.51	2.08
NA	-0.81	3.05
SA	+0.41	1.61
NP	+0.13	2.67
SP	-0.51	1.83
Indian	-1.95	2.48

CONCLUSIONS

Results indicate that differences between the ASST and the PSST may be attributable to skin-bulk temperature differences and possible cloud contamination in either or both the PSST and the ASST. It is unlikely that differences in sampling alone can account for mean differences that may exceed 3 degrees. Both the ASST and the PSST have a mean global bias that is colder than the in-situ data taken directly from the Pathfinder Matchup Database. Such a cold bias indicates possible skin-bulk temperature differences, especially with the ASST, where the global mean bias is -0.51. Differences between the ASST and the PSST also appear to have a time scale associated with an annual cycle. Such an annual cycle may be attributable to seasonal changes in mixing due to upwelling, and fluxes of heat. As a next step in the research it is necessary to separate the biases due to skin-bulk temperature differences and those due to

possible cloud contamination.

REFERENCES

Anyamba, E., and J. Susskind, A comparison of TOVS ocean skin and suface air temperatures with other data sets, J. Geophys. Res, 103 (C5), 10489-10511, 1998.

Emery, W. J., Y. Yu and G. A. Wick, Correcting infrared satellite estimates of sea surface temperature for atmospheric water vapor attenuation, J. Geophys. Res, 99 (C3), 5219-5236, 1994.

Evans, R. and G. Podesta, AVHRR pathfinder SST approach and results, EOS trans, 77 (46), 1996.

May, D. A., L. L. Stowe, J. D. Hawkins and E. P. McClain, A correction for Saharan dust effects on satellite sea surface temperatures measurements, J. Geophys. Res., 3611-3619, 1992.

McClain, E. P., W. G. Pichel, and C. C. Walton, Comparative performance of AVHRR based multichannel sea surface temperatures, J. Geophys.. Res., 90, 11587- 11601, 1985.

Murray, M. J., M. R. Allen and C. T. Mutlow, Global evaluation of sea surface temperature retrievals from the along-track scanning radiometer through comparison with the NOAA operational analysis, tech. rep. RAL-TR-96--60, 1996.

Podesta, G. P., S. Shenoi, J. W. Brown, R. H. Evans, AVHRR Pathfinder Oceans Matchup Database tech. rep. University of Miami 069-D001, 1997.

Schluessel, P., Emery, E., Grassl, H. and T. Mammen, On the Bulk-Skin Temperature Difference and Its Impact on Satellite Remote Sensing of Sea Surface Temperature, Journal of Geophysical Research, 95, 1990, 13341-13356

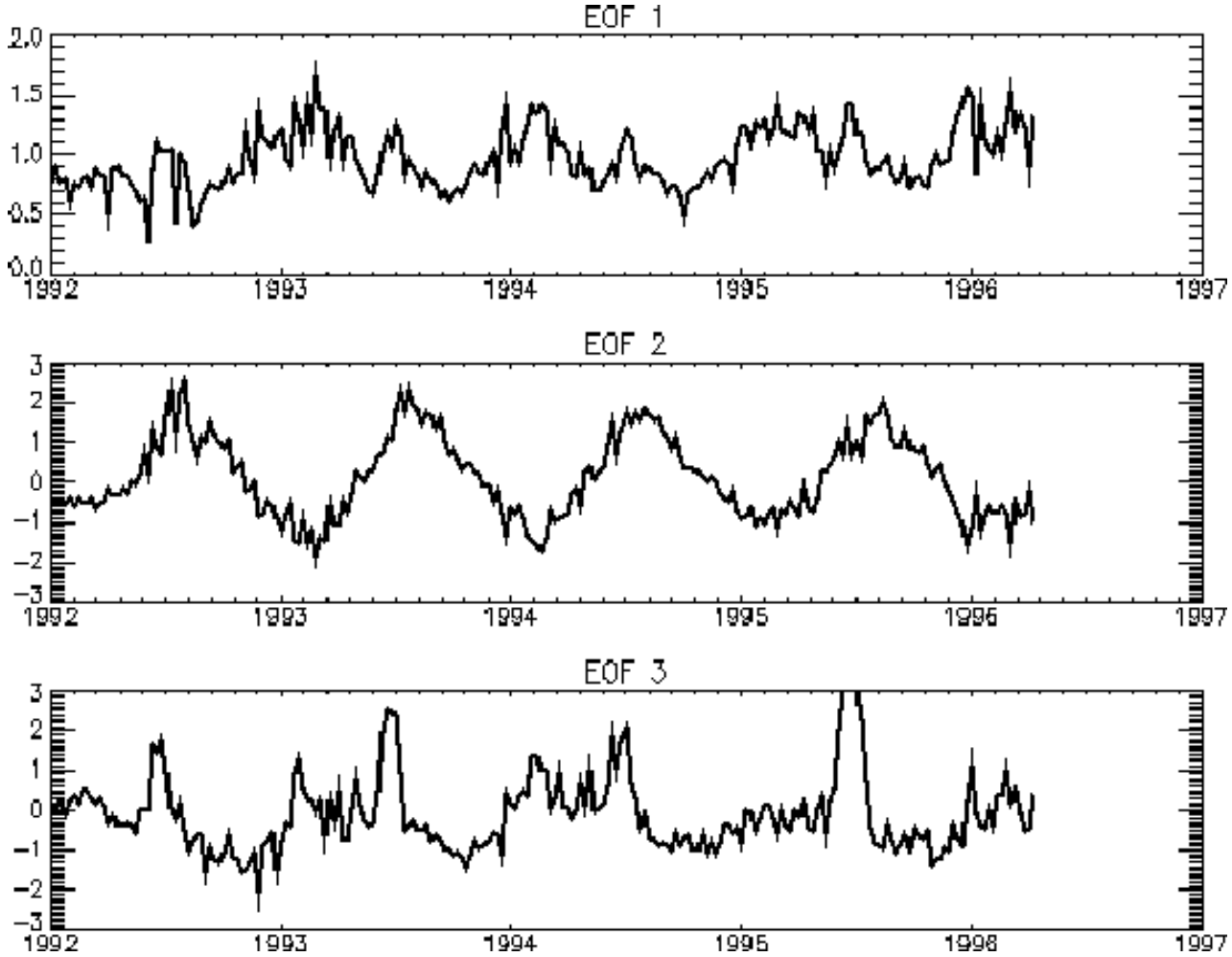

Figure 5-Time series of first three EOFs of PSST-ASST. Horizontal axis is in year from 1992-1996